scientific reports

Check for updates

OPEN

# Sensitive detection of dengue serotype-4 on lignin-derived graphene nanofibre and manganese oxide composite by DNA-sensing

Sivainesh Devi Remesh[1,2], Saravanan Karuppanan[2]✉, Veeradasan Perumal[1,2]✉, Subash C. B. Gopinath[3,4,5,6], Mark Ovinis[7], Pandian Bothi Raja[8], Natarajan Arumugam[9] & Raju Suresh Kumar[9]

**This research addresses the critical challenge of achieving precise DNA detection in complex biological samples by developing a novel, eco-friendly dengue virus serotype 4 biosensor. Utilizing laser-scribed graphene nanofibers derived from sustainable oil palm lignin, a cost-effective alternative to conventional graphene, the biosensor leverages the material's high surface area and conductivity for enhanced DNA immobilization and signal transduction. While lignin-derived graphene's heterogeneous structure poses challenges to electrochemical performance, this study overcomes these limitations by synthesizing laser scribed-graphene nanofibres (LSGNF) decorated with manganese oxide nanoparticles. Field-emission scanning electron microscopy images revealed a highly advantageous three-dimensional, interconnected network of thin, wrinkled sheets forming a porous scaffold, providing efficient electron transport and enhanced molecular interaction. Transmission electron microscopy further confirmed the successful integration of $Mn_3O_4$ nanoparticles onto the LSGNF surface. Fourier Transform Infrared Spectroscopy and Raman spectroscopy corroborated the formation of the LSGNF/$Mn_3O_4$ nanocomposite, demonstrating successful material synthesis. A dengue-specific DNA probe was then immobilized onto the nanocomposite surface, and its hybridization with complementary target DNA was evaluated. Successful DNA immobilization and hybridization were confirmed by the detection of phosphorus and nitrogen peaks using FTIR and X-ray photoelectron spectroscopy. Electrochemical impedance spectroscopy revealed the biosensor's high sensitivity, detecting dengue DNA at femtomolar concentrations ($10^{-15}$ M) with a significant decrease in impedance upon hybridization and a high signal-to-noise ratio (SNR) of 3:1, surpassing typical DNA biosensors with SNRs of 1:1 to 2:1. The biosensor exhibited excellent selectivity, optimized between SMM, TMM and NC, stability over an 8-week study, and reproducibility across five repetitive IDEs. This promising advancement in dengue diagnostics offers a faster response, improved sensitivity, and cost-effectiveness for early disease detection and management.**

**Keywords** Dengue biosensor, Laser-scribed graphene, Manganese oxide nanoparticle, Nanomaterial

[1]Centre of Innovative Nanostructures and Nanodevices (COINN), Universiti Teknologi PETRONAS, 32610 Seri Iskandar, Perak Darul Ridzuan, Malaysia. [2]Department of Mechanical Engineering, Universiti Teknologi PETRONAS, 32610 Seri Iskandar, Perak Darul Ridzuan, Malaysia. [3]Center for Global Health Research, Saveetha Medical College & Hospital, Saveetha Institute of Medical and Technical Sciences, Chennai 602105, Tamil Nadu, India. [4]Faculty of Chemical Engineering & Technology, Universiti Malaysia Perlis (UniMAP), 02600 Arau, Malaysia. [5]Institute of Nano Electronic Engineering, Universiti Malaysia Perlis (UniMAP), Kangar, Perlis 01000, Malaysia. [6]Department of Technical Sciences, Western Caspian University, Baku AZ 1075, Azerbaijan. [7]College of Engineering, Faculty of Computing, Engineering and the Built Environment, Birmingham City University, Birmingham B4 7BD, UK. [8]School of Chemical Sciences, Universiti Sains Malaysia, Gelugor, Penang 11800, Malaysia. [9]Department of Chemistry, College of Science, King Saud University, P.O. Box 2455, Riyadh 11451, Saudi Arabia. ✉email: saravanan_karuppanan@utp.edu.my; veeradasan.perumal@utp.edu.my

Dengue is a widespread virus that mostly affects tropical region with a substantial worldwide impact due to the lack of treatment and vaccine, resulting in a significant public health burden[1]. In the 2009 WHO announced severe dengue warning indicators, which have a high specificity but a low sensitivity when predicting severe outcomes in adult dengue patients[2]. This dengue severity categorization system excludes many patients, especially adults, who have dengue but do not exhibit severe symptoms[3]. Four dengue virus serotypes (DENV-1, −2, −3, and −4) are responsible for causing dengue fever[4]. These serotypes can also cause more severe forms of the disease. Protection against all four serotypes is challenging as it requires vaccines with tetravalent formulations. The live attenuated tetravalent dengue vaccine candidate (TDV) developed by Takeda has encouraging results, eliciting seroconversion to all four DENV serotypes and neutralizing antibody responses[5]. Extensive genetic variety found among DENV serotypes in DENV-4 in Bangkok, Thailand shows a high rate of evolutionary change without any indication of adaptive evolution[6]. Similarly, genotype IV of DENV-2 has taken the place of genotype V in northern India and is still in circulation, which increases the possibility of future epidemics[7].

For early diagnosis and treatment, the development of sensitive and selective diagnostic is essential. One such technique is the electrochemical DNA biosensor[8]. An important development in medical diagnostics to detect the dengue virus is the use of electrochemical biosensors that provides quick, accurate, and affordable diagnosis. The electrochemical biosensor is especially useful for on-site testing in situations with limited resources, such as those without easy access to standard laboratory facilities because of its mobility and user-friendliness[9]. Moreover, the quick turnaround time for results often only a few minutes allows for prompt clinical decision-making, which is essential for effectively controlling dengue epidemics[10]. This breakthrough has potential for a wider use in the field of infectious disease diagnostics, in addition to improving the ability for early detection and monitoring of dengue virus infections. These biosensors identify dengue viral biomarkers, such as the virus's RNA, proteins, or antibodies that the host produces in reaction to the infection[11]. They transform a biological response into an electrical signal that can be measured[12]. The dengue virus can be precisely detected even at low concentrations with high specificity due to the affinity of biological recognition elements, such as antibodies or aptamers.

Laser-scribed graphene (LSG) significantly improves electrochemical biosensors for dengue detection because of its remarkable electrical conductivity, large surface area, and simplicity of functionalization[13]. This cutting-edge substance makes creating extremely sensitive and targeted biosensors that can quickly identify dengue viral antigens easier. Proteins particular to dengue, such as antibodies, may be precisely attached because LSG is easily modifiable, enabling targeted detection for various viruses. As the production of LSG is scalable and affordable, it is ideal for developing portable, user-friendly devices for point-of-care testing, especially in situations with limited resources[14]. The incorporation of LSG into biosensors is an important technical development that provides faster and more precise dengue detection, critical for efficient patient care and epidemic containment. In addition, a major advancement in the detection of dengue viruses is the integration of manganese oxide ($Mn_3O_4$) with LSG in electrochemical biosensors. This hybrid material combines the strong electrocatalytic characteristics of $Mn_3O_4$ with the high conductivity and broad surface area of LSG, resulting in increased sensitivity and selectivity in dengue biomarkers detection[15]. The overall performance of the biosensor is enhanced by $Mn_3O_4$ capacity to promote electron transfer processes, which makes it possible to identify low amounts of viral antigens or nucleic acids quickly and precisely[16]. In addition to improving the signal response for higher detection limits, the synergistic action of $Mn_3O_4$ and LSG strengthens the biosensor's stability and longevity, increasing its dependability for point-of-care testing[17]. This novel strategy offers tremendous possibilities for early intervention and better patient outcomes in dengue-affected countries by addressing the pressing need for dengue diagnostics that are easily accessible, effective, and accurate. Despite being somewhat low in comparison to other metal oxides, MnO's isoelectric point (IEP) is essential for electrochemical dengue sensing with the use of LSG/MnO nanocomposites which is 3.1–5.1[18]. MnO nonetheless displays a pH-dependent surface charge in spite of its decreased IEP. The MnO surface becomes positively charged at pH levels lower than its IEP, which attracts negatively charged dengue-related biomolecules such as viral proteins or antibodies[19]. The adsorption of these molecules onto the LSG/MnO nanocomposite sensor is facilitated by the electrostatic attraction, which raises the concentration of target analytes at the sensor interface. As a result, the sensor's sensitivity for detecting dengue is much increased, allowing for accurate and trustworthy findings even at lower IEP levels. Moreover, MnO's low IEP did not reduce its efficacy in dengue diagnosis. The primary factor influencing the sensor's performance is its capacity to generate a surface charge that is conducive to the capture of target biomolecules. A positive surface charge is created by carefully lowering the pH of the sample solution to be below the IEP of MnO, which guarantees effective adsorption and detection of dengue-related proteins. Accurate sensing findings are made possible by this deliberate pH modification, which also offsets the reduced IEP[20].

Addressing the critical need for rapid and accurate dengue virus diagnostics, particularly in resource-limited tropical and subtropical regions experiencing significant outbreaks and lacking specific treatments or widespread vaccination, this research identifies key limitations in current biosensor technology. These limitations include achieving optimal selectivity and sensitivity, ensuring long-term stability, and enabling scalable, affordable fabrication. Recent advancements in dengue biosensor technology that leverage on the unique properties of metal oxides and their composites to achieve highly sensitive and specific detection have been thoroughly studied and tabulated in Table 1. Studies have demonstrated the efficacy of electrospun manganese(III) oxide ($Mn_2O_3$) nanofibers for electrochemical DNA nanobiosensors, achieving zeptomolar detection limits[21]. Zinc oxide (ZnO) nanorods integrated into microfluidic platforms and aluminum-doped ZnO nanostructures on interdigitated electrodes have also shown significant promise in immunofluorescence and electrochemical assays, respectively, reaching picogram/mL and nanomolar detection ranges[22]. Furthermore, the combination of laser-scribed graphene with manganese oxide ($Mn_3O_4$) nanostructures and carbonyldiimidazole-copper nanoflowers has enabled femtomolar detection through electrochemical impedance spectroscopy[23]. Table 1 These innovations

| Metal Oxide Material/Structure | Detection Method | Target Analyte | Detection Limit | Limitations | Ref |
|---|---|---|---|---|---|
| Manganese (III) oxide nanofiber | Electrochemical (CV, DPV, EIS) | Dengue DNA | 120 zeptomolar | Low conductivity of metal oxides, volume expansion | 21 |
| Zinc Oxide nanorod | Immunofluorescence | DENV-3 | $3.1 \times 10^{-4}$ ng/mL | Potential for aggregation, surface modification complexity | 22 |
| Aluminium nanoparticle doped zinc oxide | Electrochemical | Dengue Serotype 2 | 55.54 μA $nM^{-1}$ $cm^{-2}$ | Requires controlled doping, complex fabrication process | 55 |
| $Mn_3O_4$ Tetrahedral with Carbonyldiimidazole Nanoflower | Electrochemical (EIS) | DENV-4 | 1fM | Graphene restacking, complex multi-component synthesis | 23 |

**Table 1**. Selected metal oxides and their application to electrochemical biosensors for detection of dengue.

highlight the potential of tailored metal oxide nanostructures and their integration with advanced materials and microfluidic systems for early and accurate dengue diagnosis.

The integration of $Mn_3O_4$ with LSGNF in an electrochemical biosensors is a major advancement for the detection of dengue viruses. This hybrid material combines the strong electrocatalytic characteristics of $Mn_3O_4$ with the high conductivity and broad surface area of LSGNF, resulting in increased sensitivity and selectivity in dengue biomarkers detection[15]. The overall performance of the biosensor is enhanced by $Mn_3O_4$ capacity to promote electron transfer processes, which makes it possible to identify low amounts of viral antigens or nucleic acids quickly and precisely[16]. In addition to improving the signal response for higher detection limits, the synergistic action of $Mn_3O_4$ and LSGNF strengthens the biosensor's stability and longevity, increasing its dependability for point-of-care testing[17]. This strategy offers tremendous possibilities for early intervention and better patient outcomes in dengue-affected countries by addressing the pressing need for dengue diagnostics that are easily accessible, effective, and accurate.

One of the primary challenges in developing this lignin-derived graphene biosensor for dengue detection lies in ensuring its long-term stability and reproducibility in real-world diagnostic scenarios. While the novel synthesis of LSGNF/$Mn_3O_4$ offers significant advantages in sustainability and cost, maintaining consistent performance over extended periods and across different fabrication batches remains critical. Furthermore, optimizing the sensitivity and selectivity to distinguish between all dengue serotypes (DENV-1, DENV-2, DENV-3, and DENV-4) and cross-reactivity with other common viral infections presents another significant hurdle. The complexity of real biological samples, which contain numerous interfering substances, necessitates rigorous validation to ensure accurate and reliable detection[2425].

Looking ahead, this research opens several exciting avenues for future development. A significant prospect involves integrating the developed biosensor into a portable, user-friendly, point-of-care (POC) diagnostic device. This would necessitate further miniaturization, robust packaging, and the development of intuitive readout systems for rapid, on-site detection in resource-limited settings. Expanding the detection capability beyond dengue serotype 4 to encompass all serotypes, or even multiplexed detection of multiple pathogens, represents another crucial future direction[10]. Moreover, exploring the adaptability of this sustainable lignin-derived graphene platform for other medical diagnostics or environmental monitoring applications could unlock its broader potential, paving the way for a new generation of eco-friendly and cost-effective biosensors[2627].

There is a potential in utilizing sustainable and cost-effective materials like oil palm lignin for high-performance bioelectrodes, as conventional graphene synthesis methods are energy-intensive and can damage the material's structure. In this work, a highly sensitive and selective electrochemical biosensor for dengue detection by utilizing a novel hybrid nanocomposite of oil palm lignin-derived laser-scribed graphene nanofibers and hydrothermally synthesized nano-octahedral $Mn_3O_4$ nanoparticles was developed. Specifically, an in-plane biosensor with interdigitated electrodes was constructed using a lignin-polyimide precursor and a single-step laser lithography process. A one-step sol-gel hydrothermal growth method, employing manganese acetate as the seed solution and manganese nitrate as the growth solution, was used to synthesize $Mn_3O_4$. This approach enables direct growth of $Mn_3O_4$, maintaining its octahedral structure and enhancing adhesion, onto the in-plane functionalized LSG biosensor electrodes. To our knowledge, this is the first reported instance of directly producing $Mn_3O_4$ NPs on a lignin-based LSG electrode for biosensor applications and it'll be a novel approach as well[14]. Despite the potential of graphene-metal oxide composites, the challenges include achieving a controlled synthesis of lignin-derived graphene with tailored properties for DNA sensing and optimizing the synergistic integration of $Mn_3O_4$ with this graphene for enhanced electrochemical performance. This study examines the DNA immobilization and hybridization dynamics of this novel composite bioelectrodes. These include characterizing the lignin-derived LSGNF, synthesizing and characterizing the LSGNF/$Mn_3O_4$ composite with controlled properties, and optimizing DNA immobilization and hybridization on this bioelectrode to achieve enhanced detection limits. This research is novel in its utilization of oil palm lignin, an abundant agricultural waste, possesses desirable properties such as high phenolic content, inherent biocompatibility, and a rich source of functional groups, making it a promising precursor for sustainable nanomaterial synthesis[14]for graphene synthesis via cost-effective laser scribing and the direct growth of nano-octahedral $Mn_3O_4$ onto LSGNF for biosensor applications. The significance lies in the potential to develop a sustainable, affordable, and highly effective point-of-care diagnostic tool for dengue. Specifically, the LSGNF/$Mn_3O_4$ nanocomposite enables enhanced sensitivity and selectivity over existing biosensors due to its increased surface area and synergistic electrochemical properties, allowing for more efficient DNA hybridization and signal transduction (Supplementary schematic). This leads to earlier intervention, improved patient outcomes, and better epidemic control in affected regions. The entire process, from optimizing lignin-derived graphene production and the controlled synthesis of the LSGNF/$Mn_3O_4$ composite, through comprehensive material characterization, to

the fabrication and rigorous electrochemical testing of the DNA biosensor for dengue serotype 4, including sensitivity, selectivity, stability, and reproducibility assessments, is described.

## Methodology

### Materials

The lignin was extracted from empty fruit bunch oil palm[28]and polyimide film was provided by Dye Solar Cell Laboratory, Centre of Innovative Nanomaterials and Nanodevices, Universiti Teknologi PETRONAS. Manganese (II) Acetate Tetrahydrate ($Mn(CH_3OO)_2{\cdot}4H_2O$, Hexamethylenetetramine, HMT ($C_6H_{16}N_2$), and Manganese (II) Nitrate Tetrahydrate $Mn(NO_3)_2{\cdot}4H_2O$ were purchased from Sigma-Aldrich (USA), and Ethanol ($C_2H_5OH$) and Monoethanolamine, MEA ($C_2H_7NO$) were purchased from R&M chemicals (Malaysia). First Base Chemicals' phosphate buffer saline (10 mM PBS, pH 7.4) was utilized to create, wash, dilute, and serve as an electrolyte for capacitance tests. The oligonucleotide sequences used in this investigation had the following specifics: probe DNA (p-DNA): 5'-amine-$C_6$-C TTCCAC CAGGAGTACAGCTTCCTC-3'; complementary target DNA (t-DNA): 5' -GAGGAAGCTGTACTCCTGGTGGAAG- 3'; non-complementary target DNA (nc-DNA): 5'-ATGAAG CTGTAGTCTCACTGGAAGG-3'; one base mismatched target DNA (m-DNA): 5' -GAG GAAGCTGTAGTCCTGGTGGAAG- 3'; three base mismatched target (tm-DNA): 5' -GAG GAAGCTGTTGA CCTGGTGGAAG- 3' were purchased from Sigma-Aldrich (USA).

### Fabrication of LSG electrode

A 20% v/v lignin solution was evenly spread onto a polyimide sheet using the doctor's blade technique. The lignin-coated sheet was baked for one hour at 50 °C to dry. Subsequently, a $CO_2$ laser (V-460, Universal Laser System) was used to engrave the cured sheet at 300 mm/s and 21 W. The coated substrate darkens upon laser scribing, an indication that graphene has formed through the carburization process. The resulting decarbonized lignin layer was removed by immersing the sheet in a water bath. Finally, the laser-scribed graphene (LSG) electrode derived from lignin was dried at 50 °C[14].

### Preparation of LSGNF/$Mn_3O_4$

A 0.2 M $Mn(C_2H_3O_2)_2{\cdot}4H_2O$ seed sol-gel was prepared in 50 ml of ethanol[29]. This solution was heated to 60 °C and stirred at 800 rpm for 30 min. MEA was gradually added to the Manganese Oxide (MnO) seed solution at a 1:1 concentration ratio, resulting in a dark brown solution after a day of aging. The LSG biosensor was then spin-coated with the MnO seed solution at 3000 rpm for 20 s. The coated LSG IDE was dried for 20 min at 60 °C, followed by 10 min at 150 °C.

### Fabrication of DNA bioelectrode

A 0.5 cm2 interdigitated electrode (IDE) with six electrode pairs was designed in CorelDraw and fabricated via laser-scribing, following the parameters established in the preceding step for laser-scribed graphene nanofiber preparation.

### DNA immobilization and hybridization

$Mn_3O_4$ was used to alter the LSG IDE, to facilitate covalent bond contact with the aminated probe DNA. First, the LSG IDE was dropped with 20 µL of probe DNA solution, then incubated for 1 h. After that, target DNA was immobilized on the LSG IDE at different concentrations ranging from 1 fM to 1 nM and incubated for another 1 h for hybridization investigation. A detailed analysis was conducted on DNA sequences that were Single Mismatch (SMM) a single base pair difference between two otherwise complementary DNA or RNA strands is referred to as a single mismatch, or simply MM[30]. This kind of mutation occurs when a single nucleotide on one strand differs from the equivalent nucleotide in the other strand in terms of Watson-Crick complement. Third base Mismatch (TMM) RNA or DNA sequence has three mismatched base pairs. For example, if there are three sites on two DNA strands where the base pairs do not complement each other and non-complementary (NC) two DNA strands that don't pair with adenine (A) and thymine (T) or cytosine (C) and guanine (G) according to the normal base pairing principles. Stated differently, non-coding RNA (ncRNA) strands are devoid of the characteristic complementary sequence that facilitates the creation of a stable double helix structure via hydrogen bonding[31].

### Material characterizations

The surface morphology on microstructure of the electrode was examimed using FESEM (TESCAN CLARA, UHR SEM) and A HITACHI HT 7830 high-transmission electron microscope (HRTEM) was utilized to obtain higher magnification images of Bare LSG and LSGNF/$Mn_3O_4$ dispersed in ethanol and sonicated for 10 min before dropping on the copper grid. The structural properties and crystallization of LSG-NF were studied using Raman spectroscopy (HORIBA Jobin Yvon HR800) were and the Raman Spectra were obtained using a Raman Spectrometer (Horiba, HR800) with a 514 nm laser for excitation. The electrode's specific surface area (SSA) and pore diameter distribution were assessed using the Tristar 3020 Plus, utilizing the Barrett Joyner Halenda (BJH) model and the Brunauer-Emmett-Teller (BET) approach. The elemental composition of the electrode was evaluated using an X-ray photoelectron spectroscopy and Thermo Scientific K-X-ray Alpha photoelectron spectroscopy. The presence of functional groups in the material was investigated based on Fourier-transform infrared spectroscopy (FTIR) (Perkin Elmer Spectrum One) measurements. X-ray photoelectron spectroscopy (XPS) was employed to investigate the elemental composition of the electrode. The XPS spectra were obtained using a Thermo Scientific K-Alpha X-ray photoelectron spectrometer.

### Electrochemical characterization

Electrochemical impedance spectroscopy (EIS) measurements were performed using a 2-electrode system (Metrohm, Autolab) comprising a pair of working electrodes. EIS spectra were obtained across a frequency range of 10 mHz to 100 kHz. The interaction between target analytes and the sensor surface was determined by analyzing charge transfer resistance, double-layer capacitance, and changes in electrical impedance derived from EIS curves using equations provided in the supplementary material.

### DNA immobilization and hybridization

The IDE was modified with LSGNF/$Mn_3O_4$ to promote covalent bonding with probe DNA. A 5 µL probe DNA solution was applied to the LSGNF/$Mn_3O_4$ IDE, incubated for one hour, and then rinsed with PBS. For hybridization studies, varying concentrations of target DNA (1 fM to 1 nM) were immobilized on the IDE. Mismatched and non-complementary DNA sequences were also examined.

## Results and discussion

### Morphological analysis of bare LSG and LSGNF/$Mn_3O_4$ through field emission scanning Electron microscope and transmission Electron microscopy

The FESEM images of bare laser-scribed graphene (LSG), shown in Figs. 1a and b, reveal a highly advantageous morphology for graphene-based sensor applications. The structure exhibits a three-dimensional, interconnected network of thin, wrinkled graphene sheets, forming a porous scaffold. This interconnectedness creates a continuous conductive pathway throughout the material, facilitating efficient electron transport. The wrinkled and folded nature of the graphene sheets contributes significantly to a high surface area[32]. This large surface area provides ample sites for interactions with analytes or other functional materials, which is crucial for sensing or catalytic applications. The inherent porosity of the LSG framework allows for easy access and diffusion of molecules within the structure, further enhancing its interaction capabilities. The EDS mapping in Fig. 1f clearly confirms the presence of carbon as the dominant element, consistent with the formation of graphene. The uniform distribution of the carbon signal across the mapped area indicates successful laser scribing process, resulting in a relatively consistent homogeneous graphene structure[33].

The FESEM images of the LSGNF/$Mn_3O_4$ composite, depicted in Fig. 1c and d, showcase a modified morphology due to the integration of manganese oxide nanoparticles with the LSG framework. The underlying porous and interconnected graphene structure of LSG is still evident, providing the same advantages of continuous conductivity and high surface area. Crucially, the surface of the graphene sheets and the pores within the network are now decorated with a dense distribution of $Mn_3O_4$ nanoparticles[14]. These nanoparticles, as seen in higher magnification in Fig. 1 (d), are relatively uniform in size and are intimately associated with the graphene substrate. This close contact between the $Mn_3O_4$ and the conductive graphene network is structurally beneficial, ensuring efficient charge transfer between the two components. The EDS mapping of the composite in Figs. 1i, j, and k provides clear elemental confirmation. The presence and uniform distribution of manganese

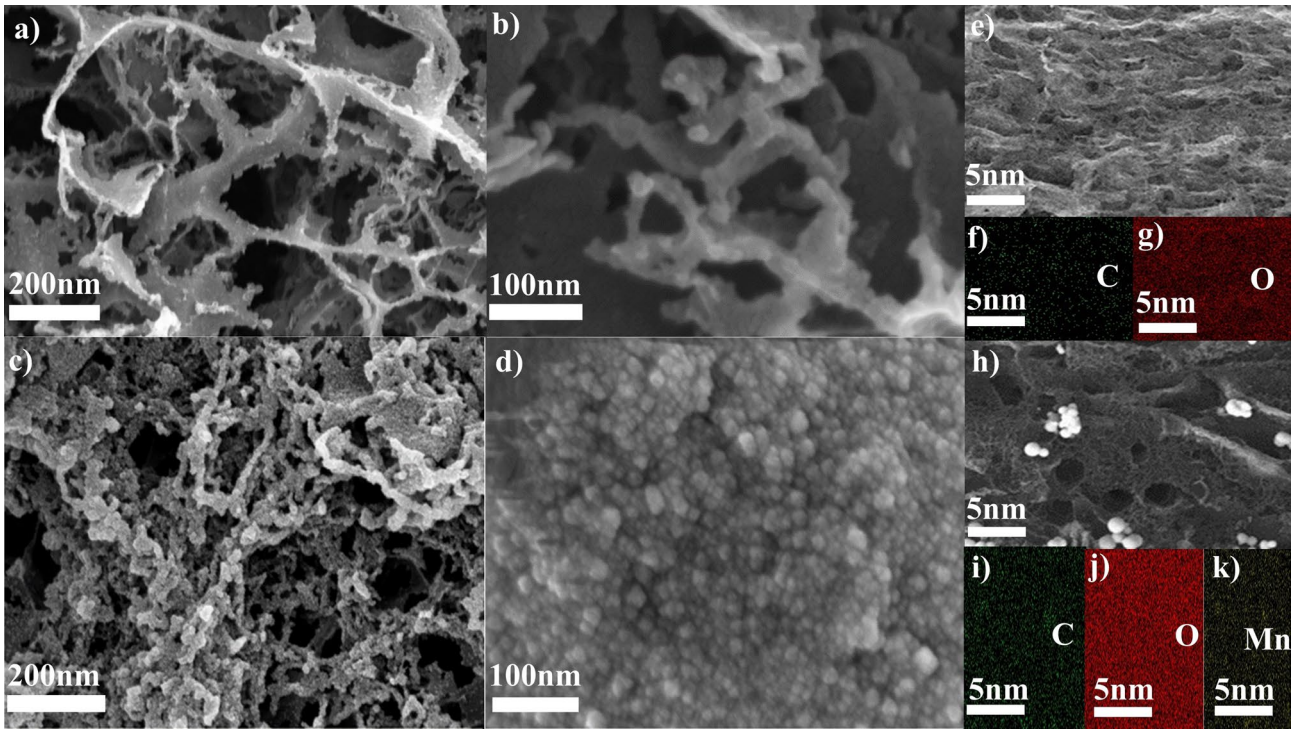


**Fig. 1**. (**a**, **b**) FESEM images of Bare LSG. (**c**, **d**) FESEM images of LSGNF/$Mn_3O_4$. (**e**–k) Elemental mapping images of Bare LSG and LSGNF/$Mn_3O_4$.

(Mn) and oxygen (O) signals, in addition to the carbon (C) signal from the LSG, confirm the successful deposition or growth of $Mn_3O_4$ onto the graphene. The spatial correlation of the Mn and O signals indicates the formation of manganese oxide, and their overlap with the carbon signal suggests a homogeneous dispersion of $Mn_3O_4$ nanoparticles throughout the LSG network[32]. This composite structure benefits from the synergistic combination of the high surface area and conductivity of the LSG with the unique electrochemical or catalytic properties of the well-dispersed $Mn_3O_4$ nanoparticles, creating a functional hybrid material with enhanced performance capabilities[14].

The Transmission Electron Microscopy (TEM) images of bare laser-scribed graphene (LSG), presented in Fig. 2a, b, and c, at increasing magnifications, reveal a morphology highly characteristic of multi-layered graphene. Figure 2a shows a large-scale view of the LSG structure, exhibiting a crumpled and folded sheet-like morphology. This morphology provides a high surface area, a significant advantage for various applications as it increases the interaction sites with other materials or analytes. Figure 2b offers a closer look, highlighting the thin, translucent nature of the graphene sheets and their interconnected, web-like arrangement. This interconnectedness establishes a continuous conductive network throughout the material, facilitating efficient electron transport, a crucial benefit for electronic and electrochemical applications. At the highest magnification, as shown in Fig. 2c, the layered structure of graphene is more clearly visible, indicating the presence of multiple stacked graphene sheets[34]. The flexibility and thinness of these layers contribute to the overall lightweight and high surface-to-volume ratio of the material, which are desirable properties for biosensing applications. FESEM and TEM analyses revealed distinct morphological differences between bare LSG and LSGNF/$Mn_3O_4$. Bare LSG exhibited a smooth, uniform surface, whereas LSGNF/$Mn_3O_4$ displayed a rougher texture with visible $Mn_3O_4$ nanoparticles dispersed on the LSG surface. TEM imaging further confirmed the successful incorporation of $Mn_3O_4$ nanoparticles onto the LSG structure with uniform size distribution. These findings collectively suggest the successful synthesis of LSGNF/$Mn_3O_4$ composite material with enhanced surface area and active sites, leading to improved catalytic performance.

To further analyze the morphological structure of the hausmannite $Mn_3O_4$ NPs produced, Transmission Electron Microscopy (TEM) images were taken, as shown in Fig. 2d–f. The TEM images of the LSGNF/$Mn_3O_4$ composite, shown in Figs. 2d, e, and f, demonstrate the successful integration of manganese oxide nanostructures with the LSG framework. Figure 2d provides a general overview, showing the LSG sheets decorated with darker, more electron-dense nanoparticles, indicating the presence of a heavier element, in this case, manganese. Figure 2e, at higher magnification, clearly illustrates the distribution of these $Mn_3O_4$ nanoparticles (highlighted by yellow circles) on the surface of the graphene sheets. The intimate contact between the nanoparticles and the underlying graphene substrate is structurally beneficial as it ensures efficient electronic coupling between the two components, potentially enhancing the overall performance of the composite material[35]. The high dispersion of the $Mn_3O_4$ nanoparticles maximizes the surface area available for interaction[34]. The high-resolution TEM image in Fig. 2f provides further confirmation of the $Mn_3O_4$ structure. The lattice fringes with a measured spacing

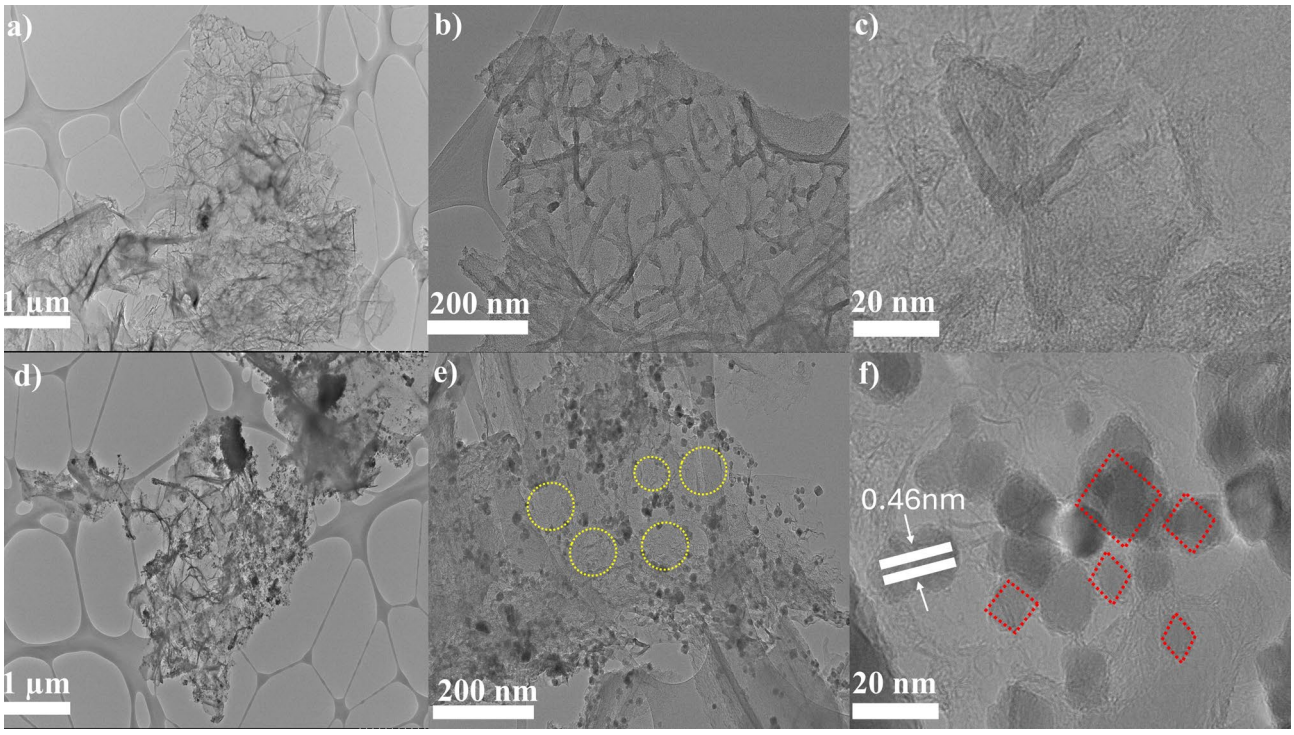


**Fig. 2**. (**a, b**) Low magnification and (**c**) High magnification TEM images of Bare LSG; inset shows overlay of imaginary cubic shapes. (**d, e**) Low magnification and (**f**) High magnification TEM images of LSGNF/$Mn_3O_4$; inset shows overlay of imaginary cubic shapes.

of 0.46 nm correspond to the crystallographic planes of $Mn_3O_4$[36]. Additionally, Fig. 2f shows the proximity and direct contact between these crystalline $Mn_3O_4$ nanoparticles (indicated by red dashed squares) and the layered graphene sheets (indicated by white lines), essential for synergistic effects in composite applications. This intimate integration allows for effective charge transfer by combining the desirable properties of both components[37].

### Crystallographic analysis of bare LSG and LSGNF/$Mn_3O_4$ through XRD

The XRD graph in Fig. 3 presents the diffraction pattern for "Bare LSGNF,". The XRD pattern of the bare LSG in Fig. 3i shows a prominent, sharp peak at approximately 26˚ (2θ). This peak corresponds to the (002) plane of graphene. The (002) peak is characteristic of the graphitic structure, indicating the stacking of graphene layers along the c-axis. The sharpness and intensity of this peak suggest a relatively ordered arrangement of graphene sheets in the laser-scribed material. The absence of other significant peaks in the bare LSG spectrum indicates that the laser scribing process primarily resulted in the formation of graphene without introducing other crystalline phases or impurities. The broadness of the base of (002) peak indicates that the graphene structure is imperfect and has some degree of disorder or defects[38,39]. The XRD pattern of the LSGNF/$Mn_3O_4$ composite reveals a more complex profile, with several distinct peaks, indicating the presence of multiple crystalline phases. In addition to the (002) peak of graphene, several peaks corresponding to $Mn_3O_4$ are observed. These peaks are indexed and labeled in Fig. 3ii. The peaks at 29.1˚, 32.3˚, 36.1˚, 38.2˚, 44.3˚, 49.3˚, 55.1˚, 60.1˚, and 64.2˚ (2θ) can be attributed to the (103), (112), (311), (222), (400), (105), (511), (440), and (553) planes of $Mn_3O_4$, respectively. These peaks confirm the presence of the $Mn_3O_4$ phase in the composite. The presence of these peaks, along with the (002) peak of graphene, indicates the successful formation of the LSGNF/$Mn_3O_4$ composite. Comparing the two spectra, it is evident that the introduction of $Mn_3O_4$ nanoparticles onto the LSG significantly altered the XRD pattern. The sharp (002) peak of graphene is still present in the composite but its intensity is reduced, suggesting that the $Mn_3O_4$ nanoparticles may have disrupted the ordered stacking of graphene layers to some extent. The presence of the $Mn_3O_4$ peaks confirms the successful incorporation of $Mn_3O_4$ onto the LSG surface[14,33].

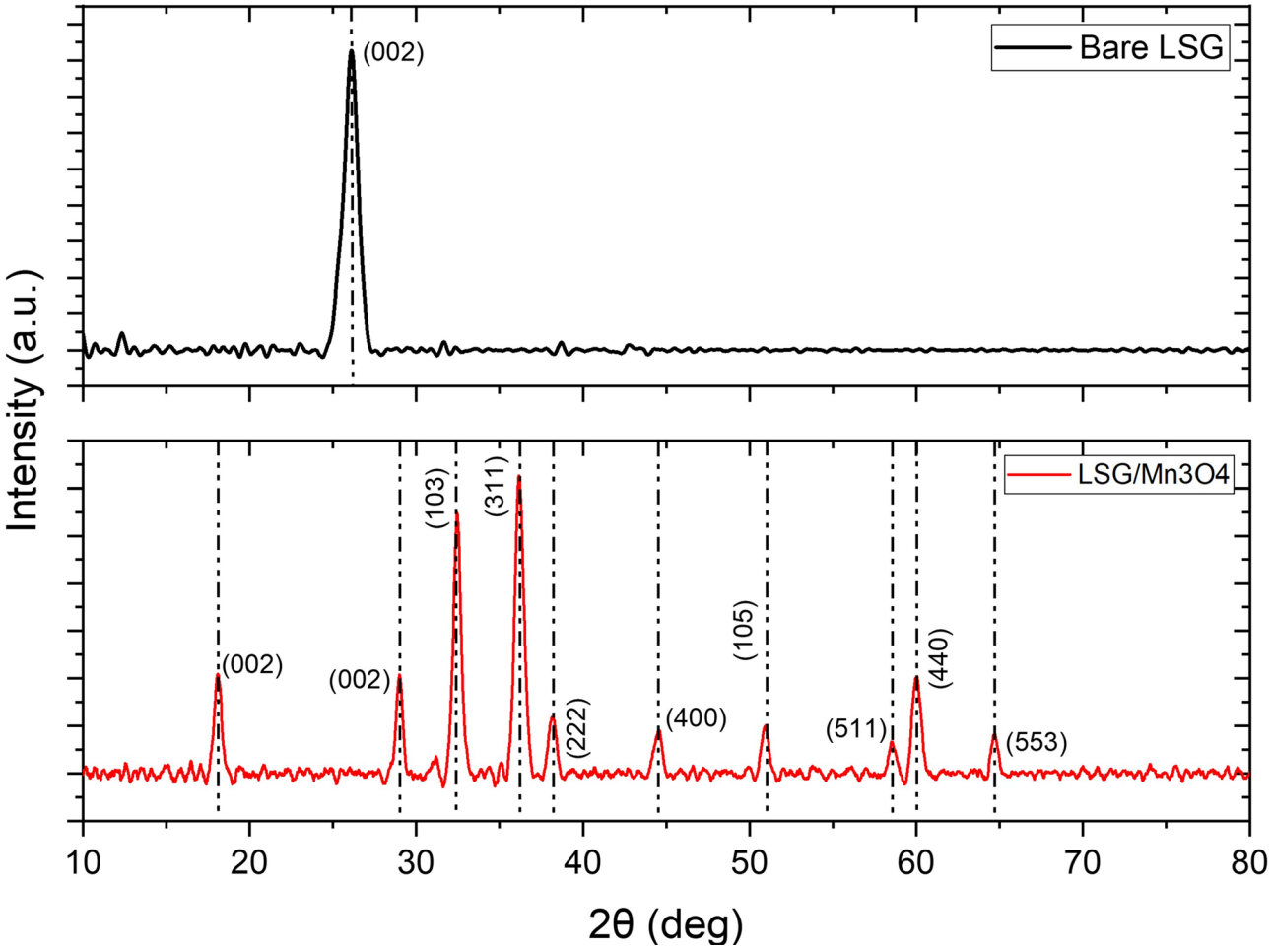


**Fig. 3**. XRD spectra of Bare LSG, (**i**) before and (**ii**) after deposition of $Mn_3O_4$.

### Optical analysis of bare LSG and LSGNF/$Mn_3O_4$ through Raman spectroscopy

The variation of graphene-based material structure encompassing disorder and defect frameworks was analyzed using Raman spectroscopy[40]. The Raman spectra of both bare LSG and LSGNF/$Mn_3O_4$ in Fig. 4(i) and (ii) reveal the stretching of the D (breath of the $sp^2$ -rings/K-point phonons of $A_{1g}$ symmetry)[41] and G (bond stretching motion of C $sp^2/E_{2g}$ phonons) bands, and the 2D band (a double-resonance process of two phonons)[42] confirming the presence of graphene in the samples[40]. The G band, located around 1586 $cm^{-1}$, corresponds to the in-plane vibration of $sp^2$-bonded carbon atoms and is indicative of the graphitic nature of the material. The 2D band, appearing around 2690–2699 $cm^{-1}$, is related to the stacking order of graphene layers and is sensitive to the number of layers. The D band, observed around 1348–1351 $cm^{-1}$, is associated with defects and disorder in the graphene lattice, such as the presence of edges, vacancies, or amorphous carbon[40]. The $A_1g$ peak, observed at 655 $cm^{-1}$ in the Raman spectrum, is a characteristic vibrational mode associated with the Mn-O stretching in $Mn_3O_4$. The presence of this peak confirms the formation of the $Mn_3O_4$ phase within the composite material. The intensity of the $A_1g$ peak at 655, while not directly provided as a ratio, indicates the presence of $Mn_3O_4$ and suggests a certain degree of crystallinity or ordered structure within the manganese oxide. The I(2D)/I(G) ratio is approximately 1.70 in both spectra. This value is generally indicative of multilayer graphene, although it does not relate to the number of layers. For monolayer graphene, this ratio is typically greater than 2, while for bulk graphite, it is closer to 0.5. The observed ratio suggests that the LSG in both samples is likely composed of a few layers of graphene[43]. The I(D)/I(G) ratio is around 0.85 for both bare LSG and LSGNF/$Mn_3O_4$. This ratio is significantly higher than 0.1, indicating a considerable defects and disorder in the graphene structure. The defects and disorder is expected for laser-scribed graphene, as the laser ablation process often introduces structural imperfections. When comparing the spectra, it was observed that the D, G, and 2D peaks are present in the bare LSG and LSGNF/$Mn_3O_4$ samples, confirming the presence of graphene in both materials. The fact that these peaks are retained in the LSGNF/$Mn_3O_4$ composite suggests that the graphene structure is largely preserved after the introduction of $Mn_3O_4$. The presence of $Mn_3O_4$ is not directly visible in the Raman spectra shown as Raman spectroscopy is more sensitive to carbon-based materials. To confirm the presence of $Mn_3O_4$, other characterization techniques like X-ray diffraction (XRD) or transmission electron microscopy (TEM) would be necessary. However, the fact that the graphene peaks are still present in the composite indicates that the $Mn_3O_4$ is likely interacting with the graphene without significantly altering its fundamental structure[42].

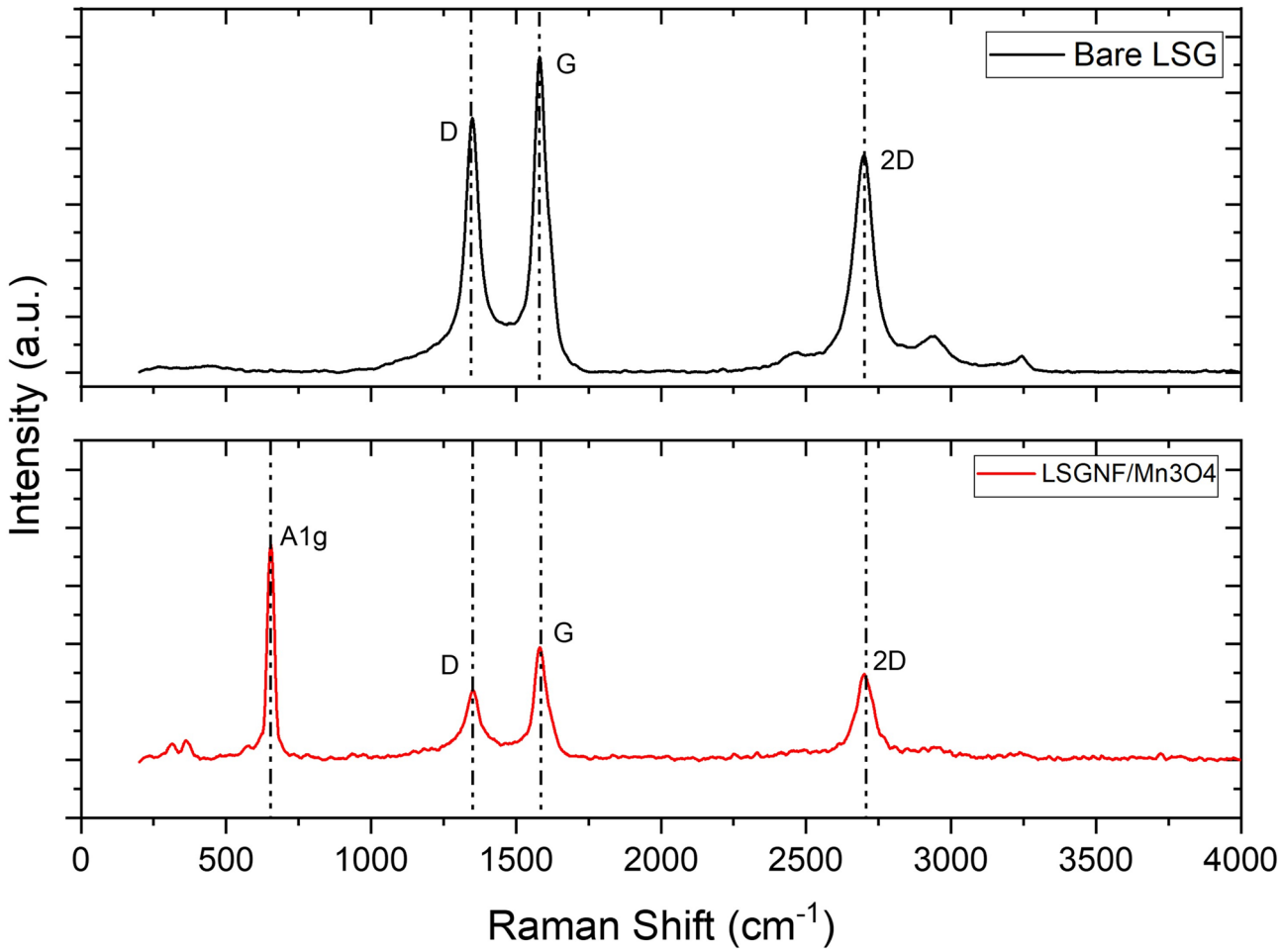


**Fig. 4**. Raman spectra of Bare LSG, (**i**) before and (**ii**) after deposition of $Mn_3O_4$.

### Validation of immobilization and hybridization through Fourier-transform infrared spectroscopy and X-ray photoelectron spectroscopy

FTIR analysis reveals the chemical composition of the LSGNF/$Mn_3O_4$ surface after probe DNA immobilization and hybridization by examining their vibrational signatures. The FTIR spectra for LSGNF/$Mn_3O_4$, immobilized probe DNA, and hybridized LSGNF/$Mn_3O_4$ (duplex) on the IDE are presented in Fig. 5(i) and (ii). In the context of a biosensor, the binding of a probe DNA to its target DNA is a fundamental process known as hybridization. This mechanism relies on the highly specific Watson-Crick base pairing rules[44]where adenine (A) always pairs with thymine (T) and guanine (G) always pairs with cytosine (C) through hydrogen bonds. The probe DNA, typically a short, single-stranded oligonucleotide with a sequence complementary to a portion of the target DNA, is immobilized on the electrode surface. When a sample containing the target DNA is introduced, if the target DNA sequence is present, it will recognize and bind to its complementary probe DNA sequence. This binding occurs due to the formation of stable hydrogen bonds between the complementary base pairs, leading to the formation of a double-stranded DNA (dsDNA) helix on the electrode surface. This highly selective molecular recognition event is crucial for the biosensor's ability to detect specific analytes[45]. The chemical bonds in functional groups attenuate infrared transmission through stretching and bending vibrations. The 700–1800 $cm^{-1}$ range is characteristic for nucleic acids[46,47]. Figure 5 compa res the FTIR spectra of immobilized (ssDNA) and hybridized (dsDNA) surfaces, showing slight differences in transmittance peaks. The peak at 54 $cm^{-1}$ and a minor vibrational band indicate deoxyribose phosphate in both probe and duplex spectra. Hybridization shifts a peak from 900 to 1250 $cm^{-1}$. Additional peaks in the 900–1250 $cm^{-1}$ range suggest increased symmetric and asymmetric vibrations of the PO43 – group in probe and target DNA, originating from the DNA phosphodiester deoxyribose backbone. Absorption peaks at 1089 and 1255 $cm^{-1}$ in both ssDNA and duplex spectra confirm the presence of DNA phosphate classes[48]. Peaks at 1450, 1640, 1738, and 1770 $cm^{-1}$, corresponding to cytosine, thymine, adenine, and guanine, respectively, confirm successful immobilization and hybridization of LSGNF/$Mn_3O_4$ on the bioelectrode[49]. The FTIR data validate the effectiveness of bioelectrode functionalization.

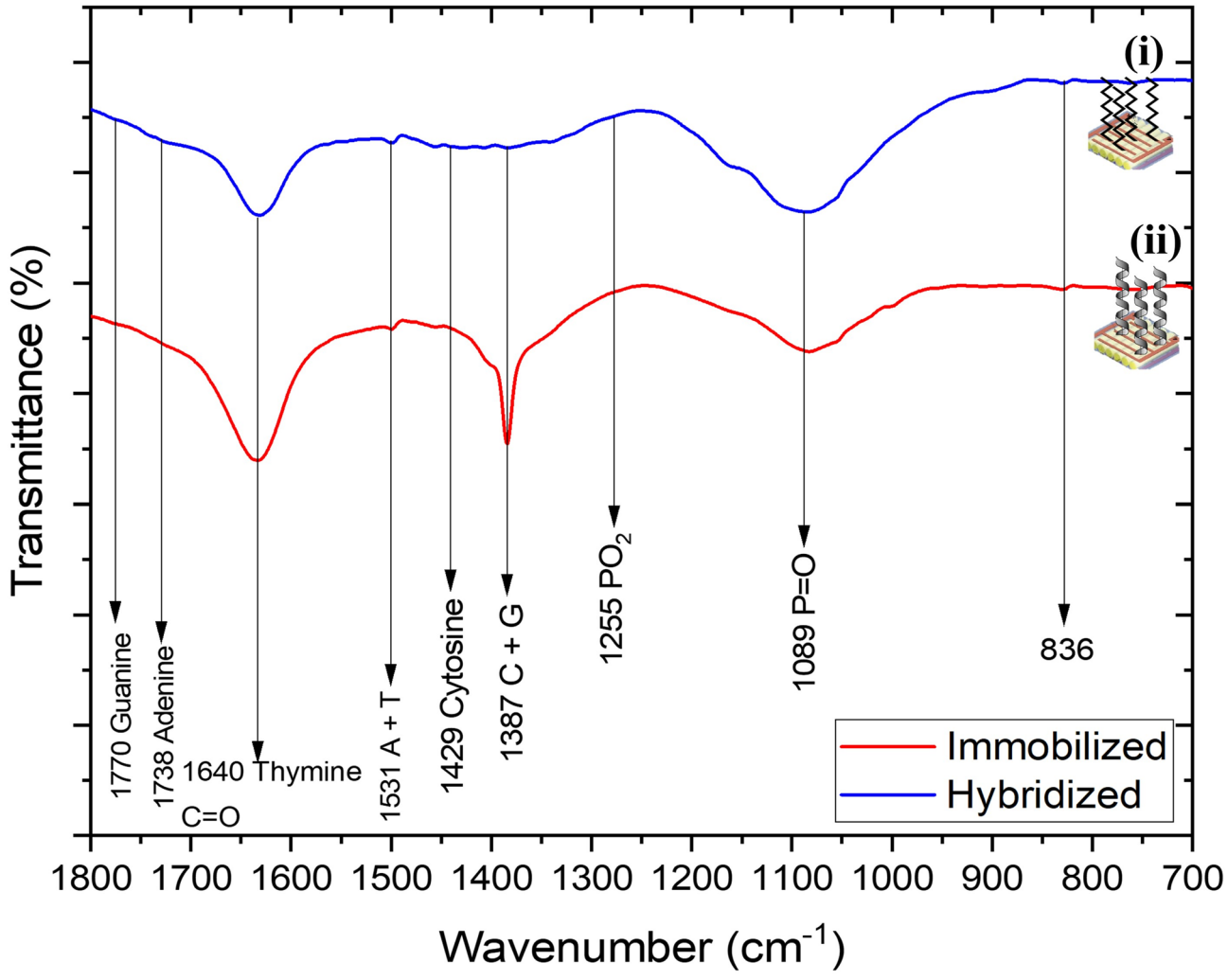


**Fig. 5**. FTIR spectra of LSGNF/$Mn_3O_4$ bioelectrode upon (**i**) immobilization and (**ii**) hybridization of DNA sequences from *Aedes Aegyptii* serotype 4. Transmittance region: 700–1800 $cm^{-1}$.

X-ray photoelectron spectroscopy (XPS) was employed to examine the elemental makeup and chemical states of the outermost layer of LSGNF/$Mn_3O_4$. Additionally, XPS was used to assess any changes on this surface after modification for *Aedes Agyptii* serotype 4 detection. Survey scans (Fig. 6) revealed carbon, oxygen, manganese, sulfur, phosphorus, and nitrogen on all three analyzed samples. Peaks at 285 eV and 533 eV were assigned to C1s and O1s, respectively, while Mn2p peaks appeared at 643 eV and 642 eV. Functionalization led to a minor increase in C1s and O1s peak intensity and a decrease in Mn2p intensity, suggesting successful immobilization and hybridization of the bioelectrode. Peaks at 165 eV and 167 eV corresponded to S2p, attributed to the thiol-terminated probe DNA. The appearance of P2p and N1s after immobilization and hybridization aligns with FTIR results showing phosphorus and nitrogen functional groups on the bioelectrode. Binding energy shifts for both immobilization and hybridization peaks further support the formation of bonds between probe DNA and target DNA on the bioelectrode surface. Therefore, XPS data confirms the bioelectrode's ability to immobilize and hybridize[29].

### Bio-sensing analyses of LSGNF/$Mn_3O_4$ nanocomposite

Electrochemical Impedance Spectroscopy (EIS) is a powerful electrochemical technique used to characterize the electrical properties of an electrode-electrolyte interface. It works by applying a small amplitude alternating current (AC) potential over a range of frequencies and measuring the resulting AC current. The impedance, which is the opposition to current flow, is then calculated as a function of frequency. This technique provides insights into various interfacial processes, including charge transfer, diffusion, and the capacitance of the electrical double layer. The double-layer capacitance (Cdl), a key parameter extracted from EIS data, arises from the accumulation of charges at the electrode-electrolyte interface, effectively acting like a capacitor[50]. Variations in Cdl are directly related to the modification of electrode surfaces. When the electrode surface is modified, for

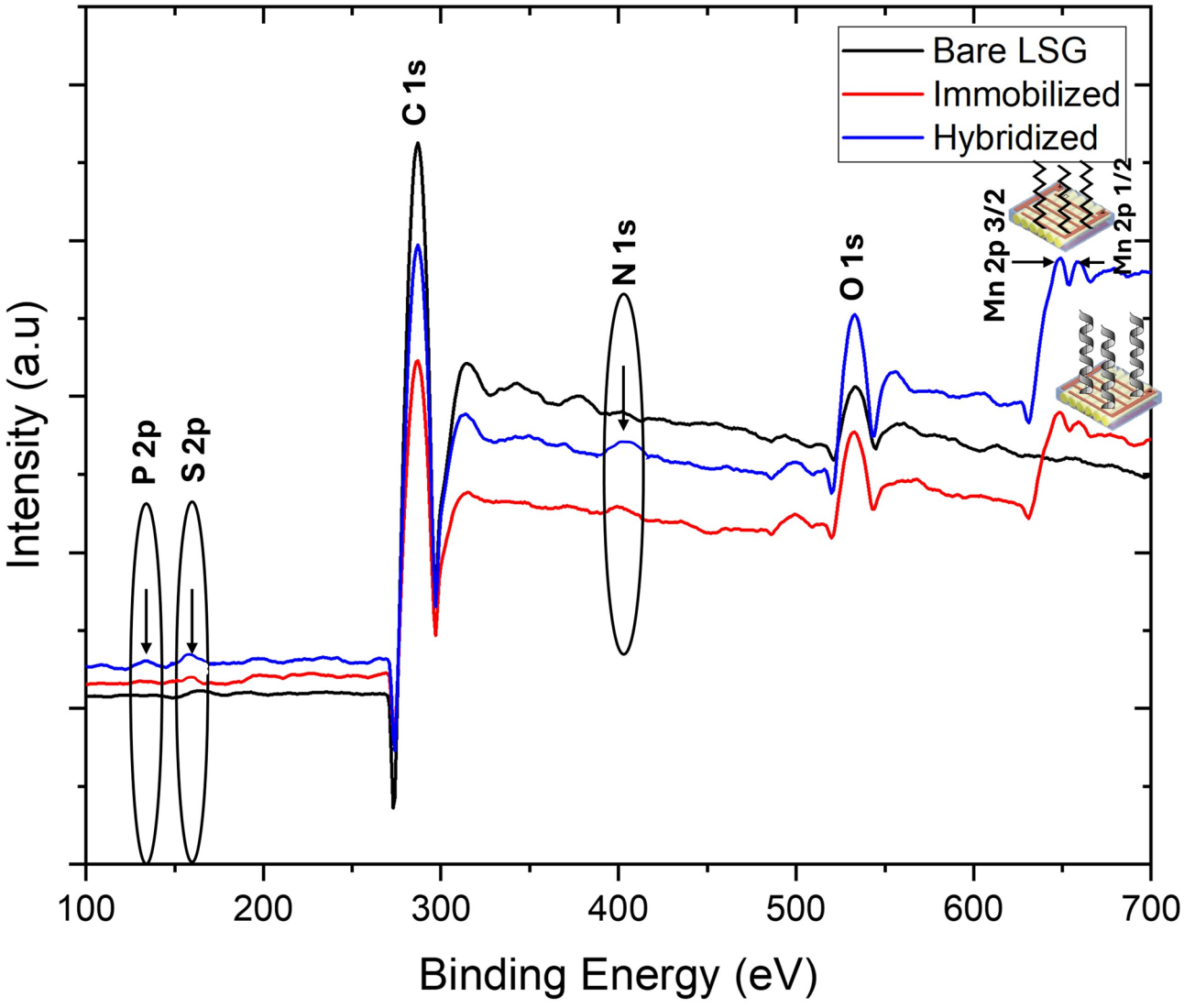


**Fig. 6**. Survey scan of XPS core level spectra for (**i**) Bare LSG, (**ii**) immobilized (LSG/LSGNF/$Mn_3O_4$/ssDNA) and hybridized (LSG/LSGNF/$Mn_3O_4$/dsDNA).

instance, by immobilizing probe DNA or upon subsequent hybridization with target DNA, the physical and chemical properties of the interface change. The introduction of biomolecules, changes in surface roughness, or alterations in hydrophobicity/hydrophilicity can all affect the amount of charge that can accumulate at the interface, thereby changing the Cdl. For example, the immobilization of DNA molecules, which are charged, can alter the ionic distribution near the electrode, leading to a change in Cdl. Similarly, the formation of a larger, more compact double-stranded DNA structure after hybridization can further impact the interfacial properties and, consequently, the Cdl value, providing an electrochemical signal indicative of the binding event[52,53].

The biosensing capability of the LSGNF/$Mn_3O_4$ decorated IDE was assessed using electrochemical impedance spectroscopy (EIS) in a 1 × PBS solution (pH 7.4). Nyquist plots were constructed from data acquired over a frequency range of 100 Hz–1 MHz (Fig. 7). These plots typically display a semicircle at higher frequencies, representing the interfacial charge transfer resistance ($R_{ct}$) related to carrier transfer from the bioelectrode to the PBS solution, followed by a linear component at lower frequencies attributed to the diffusion-limited phase. The Nyquist plot can be modeled by the Randles equivalent circuit (inset), where $R_s$ and $R_{ct}$ represent bulk solution resistance and charge transfer resistance, respectively, $Z_w$ is the Warburg impedance, and CPE is the constant phase element. In Fig. 7(a), the bare LSG exhibits a higher $R_{ct}$ (~8 Ω) due to inherent resistance to charge transfer, limited surface area, and lower conductivity. $R_{ct}$ significantly decreases (~4 Ω) after $Mn_3O_4$ growth, as $Mn_3O_4$ is a mixed-valence metal oxide with good electrical conductivity, facilitating electron transfer at the electrode-solution interface. Additionally, $Mn_3O_4$'s catalytic activity towards relevant redox reactions further lowers impedance. The steeper and shorter tail of LSGNF/$Mn_3O_4$, approaching 45°, indicates reduced Warburg resistance due to the high surface-area-to-volume ratio, increasing the electrode's active surface for electrochemical reactions[15]. $R_{ct}$ decreases to ~ 1.5 Ω after immobilization due to the negatively charged phosphate backbone of DNA attracting positive ions, creating a more conductive microenvironment. The ssDNA layer forms a partial electrical double layer, facilitating charge transfer. $R_{ct}$ increases to ~2 Ω during hybridization as dsDNA forms a more ordered and compact layer than ssDNA, creating more efficient pathways for electron transfer. Hybridization-induced conformational changes in the dsDNA layer further enhance electron transfer. Increased $R_{ct}$ is attributed to additional phosphate skeleton from target DNA, inducing more electrostatic repulsion. This confirms successful target DNA hybridization, forming a double-stranded DNA duplex on the surface. Lower impedance means faster and more efficient electron transfer, increasing sensor sensitivity. $Mn_3O_4$ and DNA modifications not only facilitate charge transfer but also amplify the signal generated by probe-target

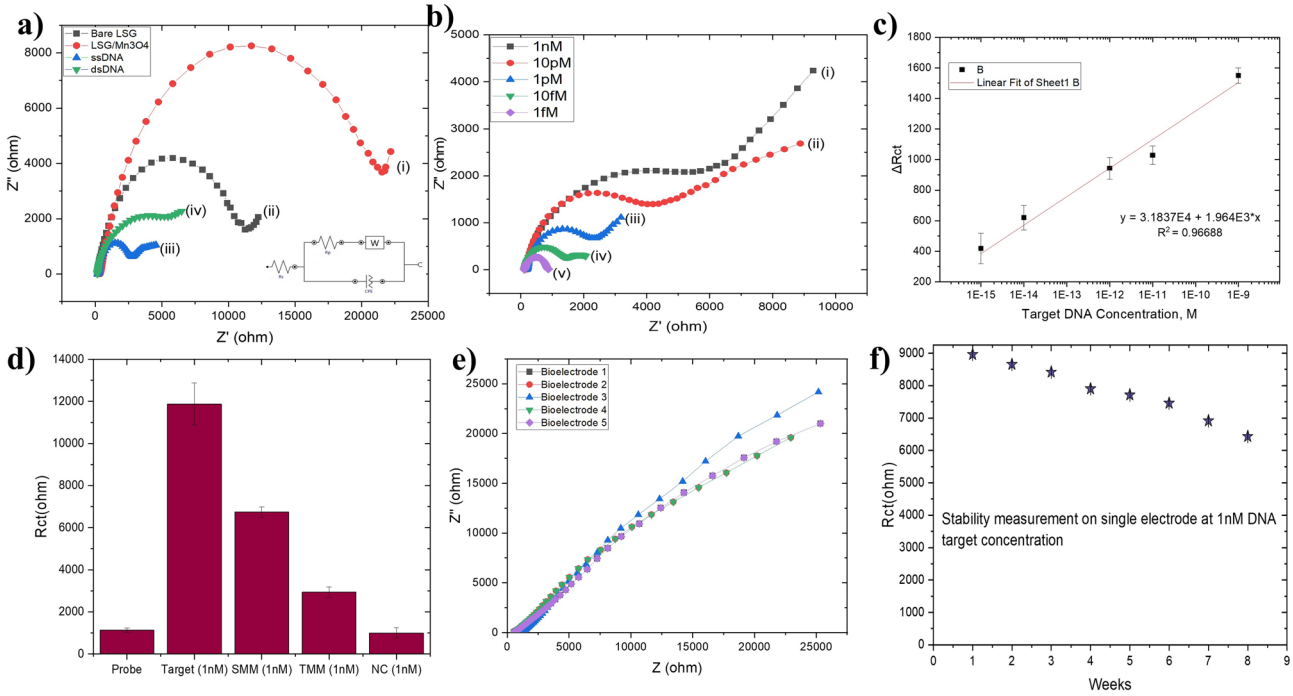


**Fig. 7**. (**a**) Impedimetric curve of (i) Bare LSG, (ii) LSGNG/$Mn_3O_4$, (ii) immobilized LSGNF/$Mn_3O_4$ (probe), and (iii) hybridized LSGNF/$Mn_3O_4$ (target) bioelectrode; the inset shows the Randles equivalent circuit, where the parameters $R_s$, $R_{ct}$, $Z_w$, and CPE represent the bulk solution resistance, charge transfer resistance, Warburg impedance, and constant phase element respectively. (**b**) Impedance spectra of LSGNF/$Mn_3O_4$ hybridized with different concentrations of complementary target DNA (i–v) 1 fM to 1 nM, (**c**) illustrates the linear regression curve at different concentrations of target DNA with the linear equation: $\Delta R_{ct} = 1.964 \times 10^3 x + 3.1837 \times 10^4$, ($R_2 = 0.96688$), (**d**) bar chart showing specificity of the LSGNF/$Mn_3O_4$ bioelectrode against mismatching and non-complementary DNA, (**e**) reproducibility curve of 5 parallel bioelectrodes fabricated under similar processing conditions, (f) stability of LSGNF/$Mn_3O_4$ biosensors.

DNA interaction, leading to a stronger signal. Specific hybridization ensures selectivity, making the sensor responsive only to the target molecule[53].

A Nyquist plot for the immobilized electrode exposed to varying target DNA concentrations (1 fM–1 nM) is shown in Fig. 7b. $R_{ct}$ increases with increasing target DNA concentrations upon hybridization due to increased electrostatic repulsion between negative ions and the negatively charged phosphate backbone in probe DNA. A linear correlation of the difference in $\Delta R_{ct}$=$R_{ct}$,hybridization−$R_{ct}$,immobilization with the logarithm of complementary DNA concentrations is shown in Fig. 7c. $\Delta R_{ct}$ increases linearly with increasing complementary DNA concentration, fitting the linear relation: $\Delta R_{ct} = 1.964 \times 10^3 x + 3.1837 \times 10^4$ with $R_2 = 0.96688$[55]. Figure 7d–f show the analytical performance of the LSGNF/$Mn_3O_4$ bioelectrode. The electrode demonstrates good linearity, with detection and quantification limits of ~ $10^{-15}$ M and ~ $10^{-13}$ M, respectively. The $R_{ct}$ for target DNA (1 nM) is ~ 12 Ω, approximately 4 times greater than the $R_{ct}$ of single-base mismatched DNA (~ 2.5 Ω) at 1 nM, indicating excellent sequence sensitivity. Non-complementary DNA shows no significant effect on $R_{ct}$ values, suggesting no specific interference. Repeatability analysis shows good reproducibility with low relative standard deviation (RSD) (Fig. 7e). The biosensor remains relatively stable with 12% degradation over 8 weeks of storage at 2 °C (Fig. 7f).

## Comparative analysis: advancements in sustainable dengue biosensors

The current research presents a significant advancement in dengue virus detection by introducing a novel, sustainable, and cost-effective in-plane biosensor. Unlike previous studies that utilized various metal oxides (like $Mn_2O_3$, ZnO, Al-doped ZnO, MnO)[21] and graphene integrated via drop-casting or deposition on complex electrode configurations such as glassy carbon electrodes or silicon-based IDEs, this work uniquely employs oil palm lignin-derived laser-scribed graphene nanofibers (LSGNF) for graphene synthesis. This eco-friendly approach not only reduces environmental impact and cost but also enables the direct fabrication of interdigitated electrodes (IDEs) on a lignin-polyimide precursor via laser lithography, simplifying the overall process. Furthermore, the direct, one-step sol-gel hydrothermal growth of nano-octahedral $Mn_3O_4$ nanoparticles directly on the LSGNF electrodes enhances adhesion and offers precise control over the nanostructure, a focused morphology not as specifically emphasized in prior research[23]. While previous studies focused on broad detection limits and various metal oxide morphologies, the current work specifically optimizes electrochemical impedance spectroscopy (EIS) for dengue serotype 4, aiming for enhanced sensitivity and selectivity through optimized DNA immobilization and hybridization on the novel LSGNF/$Mn_3O_4$ composite. This addresses previous limitations related to complex fabrication, aiming for a practical point-of-care diagnostic tool that is affordable and sustainable, directly contributing to addressing the need for accessible and efficient dengue diagnostics in resource-limited settings. This research introduces a notable advancement in dengue virus detection by leveraging sustainable oil palm lignin to synthesize laser-scribed graphene nanofibers (LSGNF), a significant departure from previous reliance on various metal oxides and graphene integration via less controlled methods. Unlike prior studies that employed diverse electrode configurations like GCE[55] or silicon-based IDEs[23]the current work streamlines the process by fabricating in-plane interdigitated electrodes directly on a lignin-polyimide precursor using laser lithography. Furthermore, while previous research explored various metal oxide morphologies (nanofibers, nanorods)[22]this study specifically focuses on the direct, one-step hydrothermal growth of nano-octahedral $Mn_3O_4$ nanoparticles onto LSGNF electrodes, optimizing electrochemical performance through enhanced adhesion and controlled nanostructure, addressing limitations such as low conductivity and aggregation seen in earlier approaches. The electrochemical impedance spectroscopy (EIS) detection method is optimized for dengue serotype 4, aiming for superior sensitivity and selectivity via advanced DNA immobilization and hybridization on the novel LSGNF/$Mn_3O_4$ composite. This emphasis on developing a practical, affordable, and sustainable point-of-care diagnostic tool directly tackles the challenges of scalable and cost-effective fabrication prevalent in earlier dengue detection methods, which often involved complex multi-step syntheses and fabrication processes. Ultimately, the utilization of agricultural waste for graphene synthesis and the direct growth of $Mn_3O_4$ on lignin-derived graphene represent a significant novel contribution towards eco-friendly and efficient biosensor fabrication for real-world applications in resource-limited settings. As a comparative study conducted for further discussion of the significance, differences, and material aspects of previous research with current research tabulated in Table 2.

## Conclusion

This research presents a novel, eco-friendly electrochemical biosensor for dengue virus serotype 4, uniquely leveraging LSGNF derived from sustainable oil palm lignin decorated with $Mn_3O_4$ nanoparticles. This represents the first reported instance of directly integrating $Mn_3O_4$ nanoparticles onto a lignin-based LSG electrode for biosensor applications, offering a cost-effective and scalable approach. Characterization confirmed a 3D interconnected LSGNF network with crystalline $Mn_3O_4$ (0.46 nm lattice spacing), validated by FESEM and TEM. FTIR and XPS confirmed successful DNA probe immobilization and hybridization via characteristic phosphorus (P2p) and nitrogen (N1s) peaks. Electrochemical impedance spectroscopy (EIS) demonstrated superior performance: $R_{ct}$ changed from ~8Ω (bare LSG) to ~4Ω (LSGNF/$Mn_3O_4$), ~1.5Ω (immobilized ssDNA), and ~2Ω (hybridized dsDNA). The biosensor achieved an ultra-high detection limit of $10^{-15}$M (femtomolar) with a 3:1 signal-to-noise ratio (SNR). It exhibited excellent selectivity (e.g., ~4-fold higher $R_{ct}$ for complementary vs. single-base mismatched DNA at 1 nM), robust stability over 8 weeks (12% degradation at 2 °C), and high reproducibility. This sustainable, highly sensitive, and selective biosensor marks a significant advancement in dengue diagnostics, promising profound impact on early disease detection and epidemic management.

| Aspect | Previous Research | Current Research | Differences | Significance | Ref |
|---|---|---|---|---|---|
| Material Synthesis and Composition | - Various metal oxides ($Mn_2O_3$, ZnO, Al-doped ZnO, MnO) synthesized through electrospinning, hydrothermal, sol-gel.<br>- Graphene integration via drop-casting or deposition | - Oil palm lignin-derived laser-scribed graphene nanofibers (LSGNF) synthesized via laser lithography.<br>- Nano-octahedral $Mn_3O_4$ synthesized via one-step sol-gel hydrothermal growth directly on LSGNF electrodes. | - Utilizes sustainable oil palm lignin for graphene synthesis, reducing environmental impact and cost.<br>- Employs a direct, one-step hydrothermal growth of $Mn_3O_4$ on LSGNF, enhancing adhesion and control over nanostructure. | Demonstrates a novel, eco-friendly approach to biosensor fabrication with improved material integration. | 21–23,55 |
| Electrode Fabrication and Configuration | - Glassy carbon electrodes (GCE), silver interdigitated electrodes (IDEs) on silicon substrates<br>- Microfluidic chip integration for some ZnO-based sensors. | - In-plane biosensor with interdigitated electrodes (IDEs) fabricated directly on lignin-polyimide precursor via laser lithography. | - Fabricates IDEs directly on a lignin-polyimide film, simplifying the process and potentially improving device miniaturization. | - Streamlines electrode production, reducing fabrication complexity and cost. | 21–23,55 |
| Metal Oxide Morphology and Properties | - Nanofibers ($Mn_2O_3$), nanorods (ZnO), nanostructures (Al-doped ZnO, MnO)<br>- Focus on enhancing surface area and conductivity | - Nano-octahedral $Mn_3O_4$ nanoparticles.<br>- Emphasis on controlled morphology and enhanced adhesion to LSGNF. | - Specific focus on nano-octahedral $Mn_3O_4$ morphology for optimized electrochemical performance. | - Highlights the importance of tailored nanostructure morphology for enhanced biosensing. | 21–23,55 |
| Detection Method and Performance | - Electrochemical (CV, DPV, EIS), immunofluorescence.<br>- Detection limits ranging from zeptomolar to femtomolar levels | - Electrochemical detection (EIS) optimized for dengue serotype 4.<br>- Aims for enhanced sensitivity and selectivity through optimized DNA immobilization and hybridization. | Focuses on optimizing DNA immobilization and hybridization on the novel LSGNF/$Mn_3O_4$ composite. | Advances the understanding of biointerface engineering for improved biosensor performance. | 21–23,55 |
| Target Analyte and Applications | - Dengue virus detection (DNA or antibodies)<br>- Focus on achieving high sensitivity and selectivity. | - Specific focus on dengue serotype 4 detection<br>- Development of a point-of-care diagnostic tool. | Aims to develop a practical, point-of-care solution, emphasizing affordability and sustainability. | Addresses the need for accessible and efficient dengue diagnostics in resource-limited settings. | 21–23,55 |
| Limitations Addressed | Low conductivity, volume expansion, aggregation, complex fabrication. | Challenges in achieving optimal selectivity and sensitivity, ensuring long-term stability, and enabling scalable, affordable fabrication. | The current study specifically targets sustainability and cost-effectiveness through lignin-derived graphene. | Demonstrates a shift towards addressing practical limitations for real-world applications | 21–23,55 |
| Novel Contributions | Various metal oxide-graphene composites for enhanced detection. | - Utilization of oil palm lignin for LSGNF synthesis.<br>- Direct hydrothermal growth of nano-octahedral $Mn_3O_4$ on LSGNF<br>- Development of a sustainable, cost-effective in-plane biosensor. | | - Demonstrates the feasibility of direct growth of $Mn_3O_4$ onto lignin derived graphene.<br>- Introduces a novel, sustainable, and cost-effective approach to dengue biosensor fabrication using agricultural waste | |

**Table 2**. A comparative analysis of dengue biosensor development of the previous and current studies.

## Data availability

No datasets were generated or analysed during the current study.

Received: 19 February 2025; Accepted: 3 July 2025
Published online: 15 July 2025

## References

1. Bhatt, S. et al. The global distribution and burden of dengue. *Nature* **496**, 504–507 (2013).
2. Thein, T. L., Gan, V. C., Lye, D. C., Yung, C. F. & Leo, Y. S. Utilities and limitations of the world health organization 2009 warning signs for adult dengue severity. *PLoS Negl. Trop. Dis* **7**, (2013).
3. Balmaseda, A. et al. SHORT REPORT: ASSESSMENT OF THE WORLD HEALTH ORGANIZATION SCHEME FOR CLASSIFICATION OF DENGUE SEVERITY IN NICARAGUA. (2005).
4. Ali, A. & Ali, I. The complete genome phylogeny of geographically distinct dengue virus serotype 2 isolates (1944–2013) supports further groupings within the cosmopolitan genotype. *PLoS One* **10**, (2015).
5. Murphy, B. R. & Whitehead, S. S. Immune response to dengue virus and prospects for a vaccine. *Annu. Rev. Immunol.* **29**, 587–619 (2011).
6. Armstrong, P. M. & Rico-Hesse, R. *EFFICIENCY OF DENGUE SEROTYPE 2 VIRUS STRAINS TO INFECT AND DISSEMINATE IN AEDES AEGYPTI*.
7. Dash, P. K. et al. Emergence and continued circulation of dengue-2 (genotype IV) virus strains in Northern India. *J. Med. Virol.* **74**, 314–322 (2004).
8. Wahala, W. M. P. B. et al. Natural strain variation and antibody neutralization of dengue serotype 3 viruses. *PLoS Pathog* **6**, (2010).
9. Thévenot, D. R., Toth, K., Durst, R. A., Wilson, G. S. & Thévenot, D. R. *Electrochemical Biosensors: Recommended Definitions and Classification*. *Biosensors & Bioelectronics* vol. 16 www. (2001). elsevier.com/locate/bios
10. Singh, A. et al. Recent advances in electrochemical biosensors: Applications, challenges, and future scope. *Biosensors* vol. 11 Preprint at (2021). https://doi.org/10.3390/bios11090336
11. Nagar, P. K., Savargaonkar, D. & Anvikar, A. R. Detection of Dengue Virus-Specific IgM and IgG Antibodies through Peptide Sequences of Envelope and NS1 Proteins for Serological Identification. *J Immunol Res* (2020). (2020).
12. Luo, X., Morrin, A., Killard, A. J. & Smyth, M. R. Application of nanoparticles in electrochemical sensors and biosensors. *Electroanalysis* vol. 18 319–326 Preprint at (2006). https://doi.org/10.1002/elan.200503415
13. El-Kady, M. F., Strong, V., Dubin, S. & Kaner, R. B. Laser scribing of high-performance and flexible graphene-based electrochemical capacitors. *Sci. (1979)*. **335**, 1326–1330 (2012).
14. Remesh, S. et al. A high performance selectively grown nano-octahedral Mn3O4 on lignin derived laser scribed graphene for microsupercapacitor applications. *J Energy Storage* **77**, (2024).

15. Zhang, W. et al. High performance Flower-Like Mn3O4/rGO composite for supercapacitor applications. *Journal Electroanal. Chemistry* **910**, (2022).
16. Yang, S. et al. Synthesis of Mn3O4 nanoparticles/nitrogen-doped graphene hybrid composite for nonenzymatic glucose sensor. *Sens. Actuators B Chem.* **221**, 172–178 (2015).
17. Danish, M. et al. Effect of soft template variation on the synthesis, physical, and electrochemical properties of Mn3O4 nanomaterial. *Inorg. Nano-Metal Chem.* **1–7** https://doi.org/10.1080/24701556.2020.1790000 (2020).
18. Kittaka, S. & Morimoto, T. *Isoelectric Point of Metal Oxides and Binary Metal Oxides Having Spinel Structure*. (1980).
19. Mu, Q. et al. Chemical basis of interactions between engineered nanoparticles and biological systems. *Chemical Reviews* vol. 114 7740–7781 Preprint at (2014). https://doi.org/10.1021/cr400295a
20. Zhang, S. et al. Assembly, and Applications of Hybrid Nanostructures for Biosensing. *Chemical Reviews* vol. 117 12942–13038 Preprint at (2017). https://doi.org/10.1021/acs.chemrev.7b00088
21. Tripathy, S., Krishna Vanjari, S. R., Singh, V., Swaminathan, S. & Singh, S. G. Electrospun manganese (III) oxide nanofiber based electrochemical DNA-nanobiosensor for zeptomolar detection of dengue consensus primer. *Biosens. Bioelectron.* **90**, 378–387 (2017).
22. Pormrungruang, P. et al. Metal oxide nanostructures enhanced microfluidic platform for efficient and sensitive Immunofluorescence detection of dengue virus. *Nanomaterials* **13**, (2023).
23. Remesh, S. D. et al. Mn3O4 tetrahedral with carbonyldiimidazole Nanoflower deposition on Laser-Scribed graphene for selective Bio-Capture. *Biotechnol. Appl. Biochem.* https://doi.org/10.1002/bab.2731 (2025).
24. Guzmán, M. G. & Kourí, G. Dengue diagnosis, advances and challenges. *International Journal of Infectious Diseases* vol. 8 69–80 Preprint at (2004). https://doi.org/10.1016/j.ijid.2003.03.003
25. Hegde, S. S. & Bhat, B. R. Dengue detection: advances and challenges in diagnostic technology. *Biosens Bioelectron. X* **10**, (2022).
26. Maluin, F. N., Hussein, M. Z. & Idris, A. S. An overview of the oil palm industry: Challenges and some emerging opportunities for nanotechnology development. *Agronomy* vol. 10 Preprint at (2020). https://doi.org/10.3390/agronomy10030356
27. Asghari, A. et al. Fast, accurate, point-of-care COVID-19 pandemic diagnosis enabled through advanced lab-on-chip optical biosensors: Opportunities and challenges. *Applied Physics Reviews* vol. 8 Preprint at (2021). https://doi.org/10.1063/5.0022211
28. Sekeri, S. H. et al. Preparation and characterization of nanosized lignin from oil palm (Elaeis guineensis) biomass as a novel emulsifying agent. *Int. J. Biol. Macromol.* **164**, 3114–3124 (2020).
29. Perumal, V. et al. 'Spotted nanoflowers': Gold-seeded zinc oxide nanohybrid for selective bio-capture. *Sci Rep* **5**, (2015).
30. Chen, S. X., Zhang, D. Y. & Seelig, G. Conditionally fluorescent molecular probes for detecting single base changes in double-stranded DNA. *Nat. Chem.* **5**, 782–789 (2013).
31. Abad-Valle, P. & Fernández-Abedul, M. T. Costa-García, A. DNA single-base mismatch study with an electrochemical enzymatic genosensor. *Biosens. Bioelectron.* **22**, 1642–1650 (2007).
32. Tai, M. J. Y. et al. Laser-scribed graphene nanofiber decorated with oil palm lignin capped silver nanoparticles: a green biosensor. *Sci Rep* **11**, (2021).
33. Loganathan, N. N., Munusamy, K. R., Perumal, V. & Pandian, B. R. Laser scribed graphene from oil palm lignin for supercapacitor applications. *J. Water Environ. Nanatechnol.* **6**, 356–366 (2021).
34. Chen, Y. et al. Enhanced electrochemical performance of laser scribed graphene films decorated with manganese dioxide nanoparticles. *J. Mater. Sci.: Mater. Electron.* **27**, 2564–2573 (2016).
35. Khan, H. A. et al. Hybrid nanoparticles of manganese oxide and highly reduced graphene oxide for photodynamic therapy. *Frontiers Bioscience - Landmark* **28**, (2023).
36. Zhang, N. et al. A novel reduction synthesis of the graphene/Mn3O4 nanocomposite for supercapacitors. *J. Solid State Chem.* **237**, 378–384 (2016).
37. Subramani, K., Jeyakumar, D. & Sathish, M. Manganese hexacyanoferrate derived Mn3O4 nanocubes-reduced graphene oxide nanocomposites and their charge storage characteristics in supercapacitors. *Phys. Chem. Chem. Phys.* **16**, 4952–4961 (2014).
38. Sun, X., Jin, H. & Qu, W. Lignin-derived 3D porous graphene on carbon cloth for flexible supercapacitors. *RSC Adv.* **11**, 19695–19704 (2021).
39. Zhang, W. et al. Lignin laser lithography: A Direct-Write method for fabricating 3D graphene electrodes for microsupercapacitors. *Adv Energy Mater* **8**, (2018).
40. Shah, H. U. et al. Hydrothermal synthesis of reduced graphene oxide-Mn3O4 nanocomposite as an efficient electrode materials for supercapacitors. *Ceram. Int.* **44**, 3580–3584 (2018).
41. Zhang, L. et al. 3D porous layered double hydroxides grown on graphene as advanced electrochemical pseudocapacitor materials. *J. Mater. Chem. Mater.* **1**, 9046 (2013).
42. Lei, Y., Alshareef, A. H., Zhao, W. & Inal, S. Laser-Scribed graphene electrodes derived from lignin for biochemical sensing. *ACS Appl. Nano Mater.* **3**, 1166–1174 (2020).
43. Popov, V. N. 2D Raman band of single-layer and bilayer graphene. in *Journal of Physics: Conference Series* vol. 682Institute of Physics Publishing, (2016).
44. Cisse, I. I., Kim, H. & Ha, T. A rule of seven in Watson-Crick base-pairing of mismatched sequences. *Nat. Struct. Mol. Biol.* **19**, 623–627 (2012).
45. Perumal, V. & Hashim, U. Advances in biosensors: principle, architecture and applications. *J. Appl. Biomed.* **12**, 1–15 (2014). https://doi.org/10.1016/j.jab.2013.02.001 Preprint at.
46. Baker, M. J. et al. FTIR-based spectroscopic analysis in the identification of clinically aggressive prostate cancer. *Br. J. Cancer.* **99**, 1859–1866 (2008).
47. Wang, L. et al. Development of an electrochemical DNA biosensor with the DNA immobilization based on in situ generation of dithiocarbamate ligands. *Bioelectrochemistry* **88**, 30–35 (2012).
48. Ramulu, T. S. et al. Nanowires array modified electrode for enhanced electrochemical detection of nucleic acid. *Biosens. Bioelectron.* **40**, 258–264 (2013).
49. Perumal, V. et al. Gold Nanorod embedded novel 3D graphene nanocomposite for selective bio-capture in rapid detection of Mycobacterium tuberculosis. *Biosens. Bioelectron.* **116**, 116–122 (2018).
50. Wang, S. et al. Electrochemical impedance spectroscopy. *Nature Reviews Methods Primers* vol. 1 Preprint at (2021). https://doi.org/10.1038/s43586-021-00039-w
51. Brett, C. M. A. Electrochemical impedance spectroscopy in the characterisation and application of modified electrodes for electrochemical sensors and biosensors. *Molecules* **27**, (2022).
52. Magar, H. S., Hassan, R. Y. A. & Mulchandani, A. Electrochemical impedance spectroscopy (Eis): Principles, construction, and biosensing applications. *Sensors* vol. 21 Preprint at (2021). https://doi.org/10.3390/s21196578
53. Rashid, J. I. A. & Yusof, N. A. The strategies of DNA immobilization and hybridization detection mechanism in the construction of electrochemical DNA sensor: A review. *Sensing and Bio-Sensing Research* vol. 16 19–31 Preprint at (2017). https://doi.org/10.1016/j.sbsr.2017.09.001
54. Zheng, J. et al. Fabricating a reversible and regenerable raman-active substrate with a biomolecule-controlled DNA nanomachine. *J. Am. Chem. Soc.* **134**, 19957–19960 (2012).
55. Al-Douri, Y., Gherab, K., Batoo, K. M. & Raslan, E. H. Detecting the DNA of dengue serotype 2 using aluminium nanoparticle doped zinc oxide nanostructure: synthesis, analysis and characterization. *J. Mater. Res. Technol.* **9**, 5515–5523 (2020).

## Author contributions

Sivainesh Devi Remesh: Conceptualization, Methodology, Writing - original draft. Saravanan Karupannan: Supervision, Project administration. Veeradasan Perumal: Project administration, Supervision, Conceptualization, Methodology. Mark Ovinis: Visualization, Validation. Subash Gopinath & Pandian Bothi Raja: Formal analysis, Validation. Natarajan Arumugam & Raju Suresh Kumar: Writing - review & editing, Validation.

## Funding

The authors gratefully acknowledge funding from YUTP (Grant No: 015LC0-443) and the efforts of the team and staff at UTP's Department of Mechanical Engineering and the Centre for Innovative Nanostructures & Nanodevices (COINN) are also acknowledged. The authors express their sincere appreciation to the Ongoing Research Funding Program (ORF-2025-143), King Saud University, Riyadh, Saudi Arabia.

## Declarations

## Competing interests

The authors declare no competing interests.

## Additional information

**Supplementary Information** The online version contains supplementary material available at https://doi.org/10.1038/s41598-025-10518-9.

**Correspondence** and requests for materials should be addressed to S.K. or V.P.

**Reprints and permissions information** is available at www.nature.com/reprints.

**Publisher's note** Springer Nature remains neutral with regard to jurisdictional claims in published maps and institutional affiliations.